Local Environment and Dynamic Behavior of Fluoride Anions in Silicogermanate Zeolites: A Computational Study of the AST Framework

Michael Fischer[a,b]

a) University of Bremen, Crystallography Group, Department of Geosciences, Klagenfurter Straße 2-4 28359 Bremen, Germany

b) University of Bremen, MAPEX Center for Materials and Processes, 28359 Bremen, Germany

E-mail: michael.fischer@uni-bremen.de

ORCID ID: 0000-0001-5133-1537

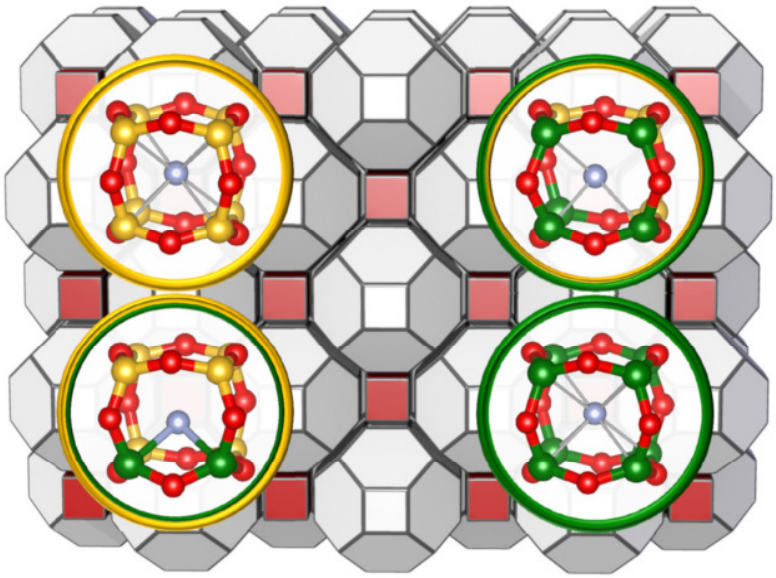

Abstract

In silicogermanate zeolites containing double four-ring (*d4r*) building units, the germanium atoms preferentially occupy the corners of these cube-like units, but the absence of long-range order precludes a determination of the preferred arrangements of Si and Ge atoms by means of crystallographic methods. If fluoride anions are present during the synthesis, they are incorporated into these cages. Due to the sensitivity of the ^{19}F chemical shift to the local environment, NMR experiments can provide indirect insights into the predominant (Si,Ge) arrangements. However, conflicting interpretations have been reported, both with regard to the preference for, or avoidance of, Ge-O-Ge linkages, and concerning the equilibrium position of fluoride inside the cage, where fluoride might either occupy the cage center or participate in a partly covalent Ge-F bond. In order to shed light on the energetically preferred local arrangements, periodic dispersion-corrected density functional theory (DFT) calculations were performed for the AST framework, which is synthetically accessible across the range of $(Si_{1-n},Ge_n)O_2$ compositions ($0 \leq n \leq 1$). DFT structure optimizations for (Si,Ge)-AST systems containing fluoride anions and organic cations revealed that arrangements of Si and Ge which maximize the number of Ge-O-Ge linkages are energetically preferred, and that fluoride tends to form relatively short (~2.2 to 2.4 Å) bonds to Ge atoms surrounded by Ge-O-Ge linkages. The preference for Ge-O-Ge linkages disappears in the absence of fluoride. DFT-based Molecular Dynamics calculations were performed for selected AST models to analyze the dynamics of fluoride anions confined to *d4r* cages. These calculations showed that the freedom of movement of fluoride varies depending on the local environment, and that it correlates with the average Ge-F distance. An analysis of the Ge-F radial distribution functions provided no evidence for a coexistence of separate local energy minima at the cage center and in the proximity of a germanium atom. The computational approach pursued in this work provides important new insights into the local structure of silicogermanate zeolites with *d4r* units, enhancing the atomic-level understanding of these

materials. In particular, the findings presented here constitute valuable complementary information that can aid the interpretation of experimental data.

1. Introduction

Sparked by the increased interest in novel porous materials for various applications (catalysis, separation, energy storage etc.), the last 20 years have seen major advances in the field of silicogermanate zeolites, neutral-framework zeolites in which the tetrahedral sites (T sites) are occupied by silicon and germanium. While a few zeolite frameworks, like AST, are accessible both in pure-SiO_2 form and as silicogermanates with various Ge contents, there are also many instances where the incorporation of Ge stabilizes frameworks that are not accessible in all-silica or aluminosilicate composition.[1] Some of these frameworks have very large pore openings, two of the most spectacular examples being the mesoporous zeolite ITQ-37, with pore apertures surrounded by 30 T atoms,[2] and ITQ-44, which possesses 18-ring pore apertures and has an exceptionally low framework density.[3] Besides efforts in the direct synthesis, it has been shown that frameworks which are composed of Si-rich sheets connected by Ge-rich building units can be disassembled through selective Ge removal, and the layers reassembled to form new materials.[4,5] This ADOR (assembly-disassembly-organisation-reassembly) approach has led to the discovery of several new zeolites that are not accessible through conventional synthesis routes.[6]

The equilibrium Ge-O-Ge angle (~130 deg) is smaller than the corresponding Si-O-Si angle (~145 deg).[7] As the formation of small (three- or four-membered) rings requires rather low T-O-T angles, the incorporation of germanium stabilizes such small rings. In particular, the presence of germanium may lead to the preferred formation of double four-ring (*d4r*) units, which are stabilized by small T-O-T angles (typically <140 degrees).[8,9] Different experimental methods have provided evidence that Ge preferentially occupies the vertices of the *d4r* cages: In favorable cases, a direct refinement of the occupancies of different T sites by Si and Ge from X-ray diffraction data is possible.[10–13] Indirect information on the Ge siting can be obtained from ^{19}F and ^{29}Si solid-state NMR experiments, and such studies have been performed – among other systems – for ITQ-7 (ISV framework),[14] ITQ-17 (BEC),[11] ITQ-13 (ITH),[15,16]

and (Si,Ge) analogues of octadecasil (AST framework).[17] Besides the experimental work, a preference of Ge for the *d4r* unit has also been found in computational modelling studies using a variety of techniques, comprising force field calculations,[9,11,12] Hartree-Fock calculations for small cluster models,[14] and periodic density functional theory (DFT) calculations.[18–20]

In systems with a mixed occupation of the vertices of a *d4r* unit by Si and Ge, the distribution of the two elements exhibits no long-range ordering, precluding a determination of preferred arrangements by means of crystallographic methods. Some information on the local ordering can be inferred from ^{29}Si-NMR spectroscopy. However, the influence of nearest-neighbor Ge atoms on the ^{29}Si chemical shift is relatively small, and contributions of several Ge atoms do not show a strictly additive behavior.[21] In zeolites synthesized via the fluoride route, fluoride anions tend to be incorporated in the smallest cage available in the structure, and they are therefore typically located in *d4r* cages if such building units are present.[22] Because the ^{19}F chemical shift depends on the composition of the *d4r* cage, ^{19}F-NMR experiments can provide insights into the local environment. It is well established that (8Si,0Ge) *d4r* cages give rise to a signal at -38 ppm (relative to $CFCl_3$),[17,23], whereas (0Si,8Ge) *d4r* cages result in a signal at ~-15 ppm[17,22] (throughout this work, we use ((8-*x*)Si, *x*Ge) as a shorthand notation to represent the occupation of the eight vertices of the *d4r* unit by 8-*x* Si and *x* Ge atoms). Other signals appearing at -20 ppm and -8 ppm in mixed (Si,Ge) systems were mostly interpreted as being due to (7Si,1Ge)/(6Si,2Ge) and (5Si,3Ge)/(4Si,4Ge) *d4r* units, respectively.[11,12,14,15,17,24–26] As an interpretation on the basis of experimental data alone may lead to ambiguities, complementary computational investigations were carried out by Sastre and co-workers: Using a combination of force field based calculations (to optimize the structures) and DFT calculations (to predict NMR shifts), they found that the computed NMR shifts for mixed (Si,Ge) systems agree much better with experiment when the F atom is not located at the center of the cage, but displaced towards a Ge atom.[26,27] For several systems, the calculations delivered pentacoordinated germanium with Ge-F bond distances in the range of 1.9 to 2.0 Å. The local environment of the pentacoordinated Ge atom, specifically the number of adjacent Ge-O-Ge linkages along edges of the *d4r* cage, was found to be a dominant factor in determining the chemical shift. This was

corroborated in recent work on STW zeolite by Rigo et al., who found three distinguishable Ge environments on the basis of a combination of NMR experiments and DFT calculations:[13] (1) "Isolated" Ge atoms surrounded only by Ge-O-Si linkages: $Ge(Ge)_0$, (2) Ge atoms surrounded by one or two Ge-O-Ge linkages along the cage edges: $Ge(Ge)_1$ and $(Ge(Ge)_2)$, (3) Ge atoms surrounded by three Ge-O-Ge linkages: $Ge(Ge)_3$ (the fourth T-O-T linkage, which has no documented impact on the NMR shift, points away from the *d4r* cage, so three is the highest possible number of Ge-O-Ge linkages along cage edges).

The AST zeolite framework was synthesized in pure-silica form by Caullet et al., who labelled it "octadecasil" to emphasize its clathrasil nature.[23] A pure-GeO_2 AST framework dubbed ASU-9 was later reported by Yaghi and Li,[28] and mixed (Si,Ge)-AST systems were prepared by Wang et al. and by Tang.[17,29] AST-type zeolites were also used as model systems in the aforementioned computational studies by Sastre and co-workers.[26,27] According to a Rietveld refinement of the GeO_2-AST end member by Wang et al., the F atoms are located at the center of the *d4r* cage, however, a large isotropic displacement factor indicates rather large freedom of motion.[17] A slight splitting of the ^{19}F-NMR signal in this system was interpreted as being due to a displacement of fluoride from the cage center, pointing to the possibility of coexisting off-center local minima, as proposed earlier by Villaescusa et al. on the basis of semiempirical calculations.[30] [29]Si-NMR results for mixed (Si,Ge) systems led to the conclusion that there is a preference for an alternating arrangement of Si and Ge, i.e. an avoidance of Ge-O-Ge linkages.[17]

To clarify the rationale behind the present work, it is useful to point out some conflicting observations in the existing literature:

(1) As discussed above, some NMR results have been interpreted as being indicative of an avoidance of Ge-O-Ge linkages, e.g. for (Si,Ge)-AST.[17] Force field based simulations on ITQ-21 and AST-type frameworks provided evidence for an energetic "penalty" for the formation of Ge-O-Ge linkages, with the relative energy increasing roughly linearly with increasing number of such linkages.[12,26] Conversely, a DFT study by Kamakoti and Barckholtz of the BEC framework delivered an arrangement in which two Ge atoms occupy adjacent cage vertices, i.e. in which a Ge-O-Ge link is present, to be the most favorable

scenario for a (6Si,2Ge) *d4r* cage.[18] A configuration with two Ge-O-Ge linkages was found to be the most stable distribution for a (5Si,3Ge) *d4r* cage. Other computational studies using electronic structure methods did not predict an energetic penalty for the formation of Ge-O-Ge linkages.[14,19] In fact, recent NMR studies on ITQ-13 and STW-type silicogermanates delivered evidence for a presence of Ge-O-Ge linkages at relatively low overall Ge contents.[13,16]

(2) Crystallographic investigations on SiO_2- and GeO_2-zeolites and mixed (Si,Ge) systems containing *d4r* units always located fluoride at the center of the cage,[12,17,23,31–33] whereas some NMR studies have pointed to an off-center displacement in Ge-containing systems.[17,30] While there is no direct experimental evidence for the presence of Ge-F bonds, the computations performed by Sastre and co-workers, which were validated against experimental NMR data, predicted the existence of pentacoordinated germanium atoms in both GeO_2-AST (d(Ge-F) ≈ 2.2 Å) and in mixed (Si,Ge) systems (d(Ge-F) ≈ 1.9 to 2.0 Å).[26,27,34]

To address the first point, structure optimizations using dispersion-corrected DFT were performed for models of (Si,Ge)-AST across the full compositional range. AST was chosen as a convenient model due to its relative simplicity (two non-equivalent T sites, 20 T atoms in the conventional unit cell, Figure 1) and due to the fact that it is synthetically accessible for essentially any Ge content. Calculations were performed for structure models including fluoride anions and tetramethylammonium cations, dubbed (TMA,F)-AST, and for models of the bare AST framework. On the basis of the calculations, the energetically preferred arrangements of Si and Ge were identified, and it was attempted to establish trends regarding the preference for, or avoidance of, certain arrangements.

With regard to the second point, the structure optimizations for (TMA,F)-AST models also deliver insights into the preferred fluoride positions and, thus, the presence or absence of pentacoordinated Ge atoms. Another interesting aspect is the dynamic behavior of fluoride in the *d4r* cage: For example, it is conceivable that several local minima exist within one cage – e.g. one at the center and another one close to a Ge atom – and that fluoride atoms "hop" between minima over time. To elucidate the dynamic

behavior, DFT-based Molecular Dynamics (MD) calculations were performed for selected models of (TMA,F)-AST.

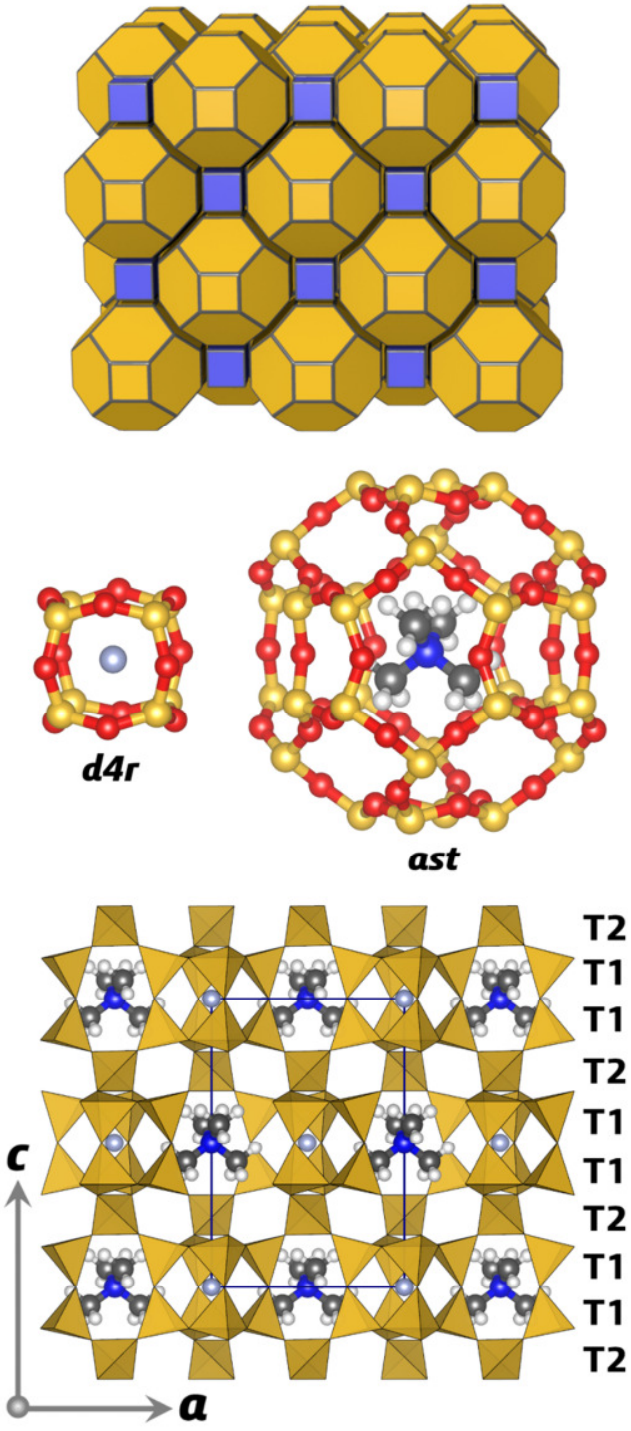

Figure 1. Top: Natural tiling representation of the AST framework. Middle: Atomistic representation of fundamental building units: *d4r* cages with fluoride anions and *ast* cages with TMA cations. Bottom: Visualization of (TMA,F)-SiO_2-AST in tetragonal space group $I\bar{4}$ (see text).

2. Models and methods

2.1 Models of AST structure

The AST framework is a relatively simple one, as it can be assembled from two types of natural tiles, namely cube-like *d4r* cages (t-cub tile, face symbol [4^6]) and larger octadecahedral *ast* cages (t-trd tile, face symbol [$4^6 \cdot 6^{12}$]).[35,36] Crystallographic investigations have established that fluorine atoms occupy the center of the *d4r* cages, whereas the organic structure directing agents (OSDAs), also called "templates", reside in the *ast* cages.[23,31] There are two distinct T sites in the structure: The T1 site corresponds to the vertices of the *d4r* cage, with the three surrounding T1-O-T1 linkages forming edges of the cage. The fourth linkage from each T1 corner forms a connection to the T2 site, which is connected to T1 sites belonging to four different *d4r* cages (Figure 1). In the cubic aristotype of AST, the T1-O-T2 linkage is linear. However, the actual symmetry of both as-made and calcined all-silica AST (octadecasil) is tetragonal (space group $I4/m$), thereby avoiding linear T-O-T linkages.[23,31,37] Tetragonal symmetry was also found for GeO_2-AST and for most mixed (Si,Ge) systems.[17,29]

The starting models used in the calculations for OSDA-containing AST included tetramethylammonium (TMA) molecules, as this is a fairly simple OSDA that has been successfully used to direct the synthesis of SiO_2-AST (octadecasil).[23,31] One complication arises, as the OSDA is disordered in the experimentally determined structure, and an ordering requires a lowering of the symmetry. Different relative orientations of the OSDA molecules in adjacent cages would lead to different resulting space groups. In the present work, an orientation was chosen that retains the body-centering of the lattice, leading to a structure in space group $I\bar{4}$ (Figure 1). While (Si,Ge)-AST and GeO_2-AST systems have not been synthesized with TMA, the reported syntheses used other alkylammonium OSDAs.[17,29] In addition to the pure-SiO_2 and pure-GeO_2 end members, models with Ge contents *n*(Ge) ranging from 0.1 to 0.9 were prepared. These models do no longer possess tetragonal symmetry (unless in very few special cases), but it was assumed that the body centering is preserved, i.e. the *d4r* units at the center and at the corners of the pseudo-tetragonal unit cell have an identical arrangement of Si and Ge. The arrangements considered, which were

generated for a model of a single *d4r* cage using the Supercell code,[38] are visualized in Figure 2. The labelling scheme to designate these systems makes use of a) the number of Si and Ge atoms occupying the vertices of the cage, b) the point group symmetry of the (Si,Ge) arrangement, and c) the number of Ge-O-Ge linkages (this is dropped from the label if there is only one (Si,Ge) distribution). For example, AST_(4Si,4Ge)_C_{4v}_4GeGe has 4 Si and 4 Ge atoms at the vertices of the *d4r* cages, which are arranged in a way that the point group symmetry of the (Si,Ge) distribution is C_{4v} – this corresponds to an occupation of all corners of one face by Ge, and therefore 4 Ge-O-Ge linkages (the edges of that face). According to Kamakoti and Barckholtz's study of BEC, an occupation of up to 4 T sites per *d4r* unit by Ge is energetically favorable. Beyond that, other T sites are occupied. To account for a possible occupation of the T2 site by germanium, comparisons between models in which T2 is occupied either by Si or by Ge were made for compositions ranging from n(Ge) = 0.5 (10 Si and 10 Ge per unit cell) to n(Ge) = 0.8 (4 Si and 16 Ge per unit cell). T2 = Si was assumed for n(Ge) up to 0.4 and T2 = Ge for n(Ge) = 0.9. A mixed occupancy of the T2 site by Ge and Si was not considered. If the T2 site is occupied by Si, it is omitted from the label (except in the case of AST_(0Si,8Ge)_O_h_T2Si), but if it is occupied by Ge, the designator "T2Ge" is appended to the label.

We have to note that the symmetry of (TMA,F)-AST, which is tetragonal, is reduced with respect to the cubic aristotype. Therefore, the *d4r* cages possess two different types of edges (T-O-T linkages), along the tetragonal *c*-axis and perpendicular to it. If this was accounted for in the setup of the model systems, a larger number of configurations than those shown in Figure 2 would arise. For example, two neighboring Ge atoms in the AST_6Si_2Ge_C_{2v}_1GeGe model could be linked along *c* or perpendicular to *c*. Test calculations for a few models indicated that the energy differences between such different configurations are small, and therefore only one arrangement of Si and Ge at the cage vertices was considered for each case. It has to be noted that different observations were made in a DFT study of BEC by Kamakoti and Barckholtz.[18] However, in that system, the T-O-T angles at the edges of the *d4r* unit vary considerably, and the occupancy of neighboring T sites by Ge is energetically favored when they are connected via a "deformable" T-O-T linkage, i.e. a link that allows the formation of a small T-O-T angle. Though not

equivalent by symmetry, the T-O-T angles at all edges of the *d4r* cages of SiO_2-AST are very similar (138 to 141 degrees).

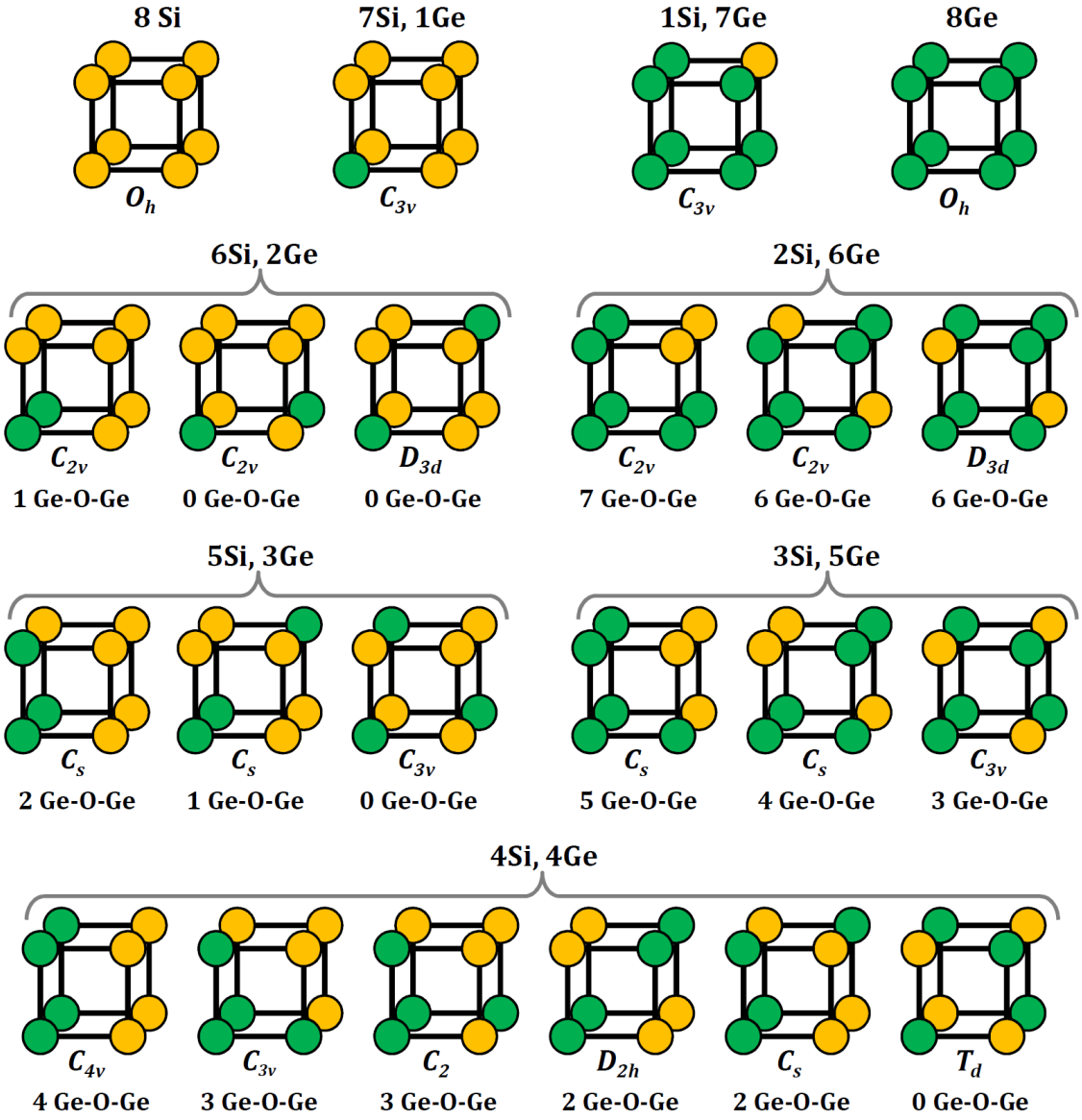

Figure 2. Visualization of (Si,Ge) distributions at the vertices of a *d4r* unit.

2.2 Computational details

DFT structure optimizations and DFT-based MD calculations were performed using the CP2K code (version 2.6.2, installed on the HLRN supercomputer "Konrad"), which uses a hybrid Gaussian and plane wave scheme.[39,40] All calculations used the PBE exchange-correlation functional in conjunction with the "Grimme-type" D3 dispersion correction,[41,42] a plane wave energy cutoff of 600 Ry, and Goedecker-Teter-Hutter pseudopotentials devised by Krack.[43] Only the gamma point was used to sample the first Brillouin zone. All calculations used Gaussian "MOLOPT" basis sets that are included in the current distribution of CP2K:[44] The structure optimizations used triple-zeta (TZVP) basis sets, as it was found that these give a much more accurate difference in lattice energy between SiO_2-AST and quartz than double-zeta (DZVP) basis sets (TZVP: 11.6 kJ mol^{-1}; DZVP: 16.1 kJ mol^{-1}, experiment: 10.9 kJ mol^{-1}). However, both basis sets were found to deliver very similar equilibrium structures, justifying the use of the less demanding DZVP basis in the MD simulations.

The structure optimizations were performed for the conventional unit cell of tetragonal AST. All atomic coordinates and the lattice parameters were optimized, fixing the symmetry of the lattice to tetragonal (a = b, all angles = 90 degrees). The optimizations used the following convergence criteria: Maximal geometry change = $2 \cdot 10^{-5}$ bohr, maximal residual force = $1 \cdot 10^{-6}$ Ha $bohr^{-1}$, maximal pressure deviation = 0.01 GPa. The MD simulations took the optimized structures as starting point and used a 2×2×1 supercell. MD simulations were performed in the canonical (*NVT*) ensemble for a temperature of 298 K, using a Nosé-Hoover thermostat with a timestep of 0.5 fs and a time constant of 50 fs. To improve the statistics, three independent trajectories were run for each system, with each trajectory consisting of an equilibration stage of 2.5 ps (5000 steps) and a production stage of 7.5 ps (15000 steps). All results presented below correspond to averages over three trajectories. For the analysis of the production part of each MD trajectory, the root mean square displacements (RMSD) of all elements and radial distribution functions (RDF) of selected pairs of elements were computed using the VMD software, version 1.9.3.[45]

3. Results and discussion

3.1 Equilibrium structures of the end members: SiO_2-AST and GeO_2-AST

Initial DFT structure optimizations were performed for the end members SiO_2-AST and GeO_2-AST, both with and without TMA template and F anions. The resulting lattice parameters are shown in Table 1, together with experimental data, where available.[17,31,37] For SiO_2-AST, the computed lattice parameters agree reasonably well with experiment, although there is a systematic tendency to overestimate the length of the *c*-axis, while underestimating *a*. Similar findings have been discussed in more detail in previous benchmarking work.[46,47] For (TMA,F)-GeO_2-AST, the *c*-axis is overestimated even more markedly. However, it has to be considered that the experimental sample contained a different OSDA than the model used in the calculations (dimethyldiethylammonium instead of TMA), and that the dimensions of the OSDA will affect the equilibrium lattice parameters.

In addition to the lattice parameters, we also evaluated the difference in DFT energy per TO_2 unit between template-free SiO_2-AST/GeO_2-AST and α-quartz/quartz-type GeO_2 (ΔE_{DFT}). This quantity can be taken as a realistic approximation to the enthalpy of transition ΔH_{trans}.[46–48] The enthalpy of transition of SiO_2-AST has been determined as 10.9±1.2 kJ mol^{-1} per formula unit using solution calorimetry experiments.[49] The DFT-calculated energy difference is within the experimental error limits, amounting to 11.6 kJ mol^{-1}. Calculations for several other all-silica zeolites and α-cristobalite, summarized in the Supporting Information (SI, Table S1), provided similarly good agreement, giving confidence in the predictions of the relative stability of AST systems, presented below. We may note that calculations using the plane-wave code CASTEP and employing similar dispersion-corrected DFT methods gave ΔE_{DFT} values in the same range: A (so far unpublished) energy difference of 10.9 kJ mol^{-1} was obtained with the PBE-D2 functional,[46] and the PBEsol-D2 functional delivered 11.4 kJ mol^{-1}.[47] The calculated ΔE_{DFT} for GeO_2-AST with respect to quartz-type GeO_2 is approximately 1.5 times as large as for the silica systems, amounting to 17.7 kJ mol^{-1}. This is in line with experimental findings, as an increase in metastability (corresponding

to larger values of ΔH_{trans}) with increasing germanium content has been observed in calorimetric experiments on silicogermanate zeolites.[50]

Table 1. Lattice parameters and unit cell volumes of pure end members, SiO_2- and GeO_2-AST, as obtained from DFT calculations, and comparison to experimental values (where available).

		a / Å	*c* / Å	*V* / Å^3
(TMA,F)-SiO_2-AST	DFT	8.970	13.605	1094.7
	Exp[31]	9.068	13.438	1105.0
SiO_2-AST	DFT	9.122	13.727	1142.2
	Exp[37]	9.255	13.501	1156.4
(TMA,F)-GeO_2-AST	DFT	9.151	14.635	1225.5
	Exp[17]	9.271	14.349	1233.3
GeO_2-AST	DFT	9.074	14.505	1194.3

In the (TMA,F)-systems, the fluoride anions occupy the center of the *d4r* cages, as shown in Figure 3 a and b. Due to the longer bond length of Ge-O bonds in comparison to Si-O bonds, this cage has larger dimensions in (TMA,F)-GeO_2-AST, with an edge length of ~3.24 Å and a body diagonal of 5.62 Å, compared to (TMA,F)-SiO_2-AST with dimensions of ~3.05 Å and 5.30 Å, respectively. As noted above, a central position of fluoride has been observed in various crystallographic studies of as-synthesized zeolites containing *d4r* units, and in molecular, anionic *d4r*-like $[T_8O_{12}(OH)_8F]^-$ units.[30,51,52] High-level wave-function based calculations for these molecular systems pointed to a moderately strong non-covalent interaction ("tetrel bonding"), but no off-center displacement of fluoride.[53] On the contrary, both force field and DFT-PBE calculations by Sastre and Gale for as-synthesized GeO_2-AST predicted a displacement of F towards one Ge atom, with a Ge-F distance of ~2.17 Å, indicating a significant covalent bonding component.[34] These contrasting findings could indicate the presence of different local minima within one cage, a point to which we return in the context of the MD calculations.

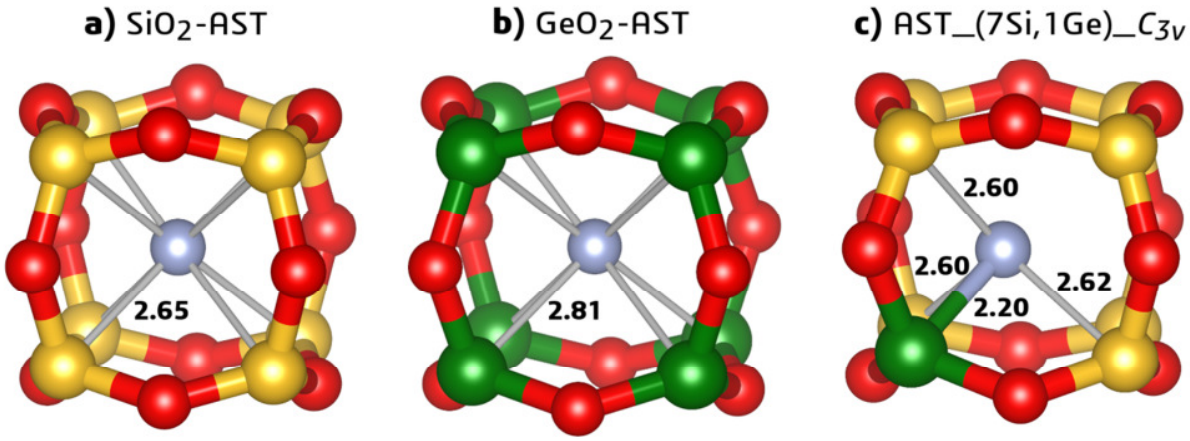

Figure 3. Fluoride environment in (TMA,F)-AST systems: SiO_2-AST, GeO_2-AST, and AST_(7Si,1Ge)_C_{3v}. Selected interatomic distances are given in Å.

3.2 Equilibrium structures of (TMA,F)-AST across the compositional range

With regard to (TMA,F)-AST models across the range of compositions, we first take a brief look at the evolution of the DFT-optimized lattice parameters *a* and *c* as a function of the Ge content, shown in Figure 4. As expected, both lattice parameters increase with *n*(Ge). In the composition range from *n*(Ge) = 0.5 to 0.8, there is a marked dependence on the occupation of the T2 site, with models with T2 = Ge having a longer *c*-axis and shorter *a*-axis than models with T2 = Si. Experimental values are also included in Figure 4.[17,29,31] The quantitative deviations between DFT and experiment can, at least in part, be explained with the presence of a different OSDA in all experimental samples except SiO_2-AST. It is, however, interesting to observe that the GeO_2-AST sample has a shorter *a*-axis than most (Si,Ge) systems, whereas its *c*-axis is about 0.3 Å longer than that of the most Ge-rich (Si,Ge) sample (where *n*(Ge) = 0.833). In the light of the relationships discussed above, this might indicate that the T2 site is preferentially occupied by Si even in Ge-rich samples. As we will see below, the calculations predict T2 = Si to be preferred up to *n*(Ge) = 0.7.

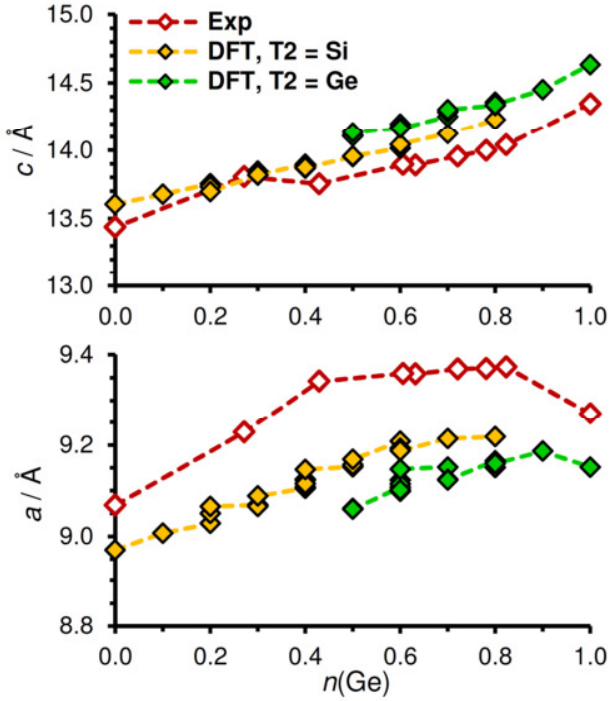

Figure 4. Evolution of lattice parameters *c* (top panel) and *a* (bottom panel) of (TMA,F)-AST as a function of germanium content. Experimental values are included for comparison.[17,29,31]

In the following, we concentrate on the relative stabilities of different (Si,Ge) distributions for a given Ge content, and on the environment of the fluoride anions in the most stable structures. To analyze this in a systematic fashion, we present the most significant findings for each composition from *n*(Ge) = 0.1 to 0.9. The relative energies and shortest Ge-F distances for all models are compiled in Table 2, and fluoride environments of selected models are shown in Figures 3, 5, and 6. In these figures, Ge-F distances of less than 2.4 Å are indicated using thick bicolor lines, like covalent bonds, whereas distances between 2.4 and 2.7 Å are represented using thin grey lines (Ge-F distances above 2.7 Å are not shown). Of course, the choice of a distance of 2.4 Å as a threshold is entirely arbitrary. In reality, there will be a more or less smooth transition between short, partly covalent Ge-F bonds and long non-covalent Ge-F contacts.

***n*(Ge) = 0.1:** In AST_(7Si,1Ge)_C_{3v}, fluoride is situated in a qualitatively different location than in the SiO_2 and GeO_2 end members discussed above (Figure 3 c), as it is located much closer to the Ge atom

than to all other vertices of the *d4r* cage, with a Ge-F distance of 2.20 Å. This pronounced displacement from the cage center indicates a degree of covalent Ge-F bonding. Upon coordination of fluoride, the coordination environment of Ge distorts away from a tetrahedral environment without reaching the bond angles of 90 and 120 degrees of a perfect trigonal bipyramid. While the Ge-O bonds in the plane perpendicular to the Ge-F bond have essentially the same length as those in GeO_2-AST (1.77 Å), the apical Ge-O bond is elongated modestly to 1.79 Å. Qualitatively, the formation of pentacoordinated Ge agrees with the previous computational predictions by Sastre and co-workers.[27] However, their calculations delivered a much shorter Ge-F distance of 1.89 Å.

***n*(Ge) = 0.2:** The fluoride environment in the optimized (6Si,2Ge) models is shown in Figure 5. Of the three distinct arrangements, the configuration in which two Ge atoms are located at adjacent vertices, forming a Ge-O-Ge link, is energetically most favorable. In this system, the fluoride anion has short contacts to both Ge atoms, with the Ge-F distances being slightly longer than that found above for AST_(7Si,1Ge)_C_{3v}. In the other two models, which are energetically less favorable by 10 and 13 kJ mol^{-1} per *d4r* unit, respectively, fluoride is also located at a similar distance from both Ge atoms, but the Ge-F distances are significantly longer.

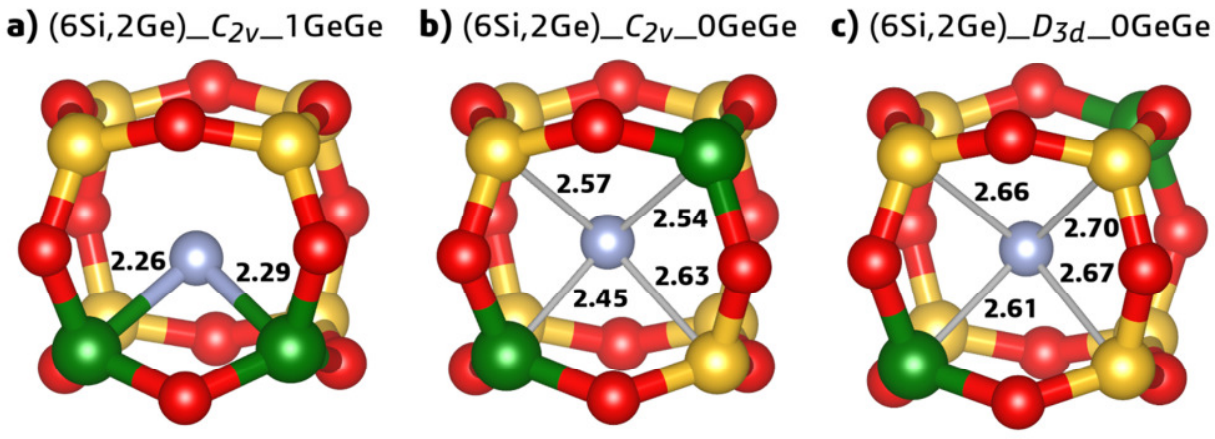

Figure 5. Fluoride environment in three (TMA,F)-AST models having *n*(Ge) = 0.2. Selected interatomic distances are given in Å.

***n*(Ge) = 0.3:** For this composition, the lowest-energy model is AST_(5Si,3Ge)_C_s_2GeGe, where one germanium atom participates in two Ge-O-Ge links. As is visible in Figure 6 a, fluoride forms a rather short Ge-F bond to this $Ge(Ge)_2$ atom, whereas the distances to the other two Ge atoms are significantly longer. Unlike in the *n*(Ge) = 0.2 case, where the energetically preferred model is the only system having a short Ge-F bond, such a bond is also found in the second best system, AST_(5Si,3Ge)_C_s_1GeGe.

***n*(Ge) = 0.4:** The complexity increases further for this composition, with a total of six distinct (Si,Ge) distributions. All in all, the tendency observed above is corroborated: The energetically most favorable model AST_(4Si,4Ge)_C_{3v}_3GeGe contains one $Ge(Ge)_3$ atom, and fluoride is bonded to this atom, with a short Ge-F distance of 2.17 Å (Figure 6 b). There is, however, a second configuration with longer Ge-F distances that is almost identical in energy. In this AST_(4Si,4Ge)_C_{4v}_4GeGe model, shown in Figure 6 c, the four germanium atoms surround one face of the *d4r* unit. The fluoride anion is displaced from the cage center towards this face, with four rather similar Ge-F distances ranging from 2.42 to 2.54 Å.

***n*(Ge) = 0.5:** This is the first composition for which models with T2 = Si and T2 = Ge were compared, in addition to considering different (Si,Ge) distributions within the *d4r* unit. The most favorable model has T2 = Si and is 5 kJ mol^{-1} lower in energy than the best T2 = Ge case. Again, it possesses the largest possible number (five) of Ge-O-Ge linkages (Figure 6 d). In this configuration, fluoride is displaced towards one of the $Ge(Ge)_3$ atoms, but the shortest Ge-F distance of 2.42 Å is notably longer than in the systems with lower Ge contents.

***n*(Ge) = 0.6:** A total of nine different models were included for this composition. As above, the model with T2 = Si and with the largest number of Ge-O-Ge linkages constitutes the energetically preferred (Si,Ge) distribution (Figure 6 e). However, two of the models with T2 = Ge are within ~1 kJ mol^{-1} of this system, so the T2 site might be partially occupied by Ge in a real system. The (Si,Ge) distribution within the *d4r* unit in these two systems corresponds to the two best models found above for the *n*(Ge) = 0.4 case, and the fluoride environments are similar to the corresponding ones for the (4Si,4Ge) models visualized in Figure 6 b and c.

***n*(Ge) = 0.7:** For this composition, only one model with T2 = Si remains, in which seven vertices of the *d4r* unit are occupied by Ge. This distribution is 1.5 kJ mol^{-1} higher in energy than a model with T2 = Ge and a distribution of Si and Ge on the vertices corresponding to that of AST_(3Si,5Ge)_C_s_5GeGe. This trend continues for ***n*(Ge) = 0.8**, where the energy difference between the preferred model and the only model with T2 = Si is increased to 2.5 kJ mol^{-1} (although still small in absolute terms). The fluoride environment in the preferred AST_(2Si,6Ge)_C_{2v}_7GeGe_T2Ge system is largely similar to that shown in Figure 6 e for the analogous T2 = Si case.

***n*(Ge) = 0.9:** As for *n*(Ge) = 0.1, only one distribution remains at this high Ge content, in which seven of the eight cage vertices are occupied by Ge. The fluoride anion is displaced from the cage center towards the Ge atom that lies at the vertex opposite the only Si atom (Figure 6 f), forming a Ge-F contact having an intermediate length of 2.38 Å.

Altogether, we can summarize the observations as follows: The calculations indicate that a progressive occupation of the available T1 positions by germanium is preferred over occupation of the T2 site up to fairly high Ge contents of ~0.6, indicating that each *d4r* cage can accommodate up to six Ge atoms at its vertices without energetic "penalty". With regard to fluoride, the formation of short Ge-F bonds (~2.2 to 2.3 Å) is preferred up to *n*(Ge) = 0.4. Such bonds are preferentially formed with Ge atoms that are linked to other Ge atoms, leading to an energetic preference for models having the largest possible number of Ge-O-Ge linkages. At higher Ge contents, fluoride occupies a more central location in the cage, but it nevertheless tends to form one fairly short contact (~2.4 Å) with a Ge(Ge)$_3$ atom.

We need to add a few words of caution to the discussion of the relative stability of different arrangements, pointing out the simplifications that – necessarily – have to be made in such a study: First of all, it has to be kept in mind that the arrangement in a real crystal structure is a result of the processes happening during hydrothermal zeolite synthesis (assembly of isolated TO_4 tetrahedra to form precursor building units followed by the connection of these building units to form the extended structure). Such a complex assembly process, which is governed by the interplay of thermodynamics and kinetics, cannot, at present,

be captured with DFT methods. While we see no reason to expect that fundamentally different preferences, especially an *avoidance* of Ge-O-Ge linkages within the *d4r* units, would be observed if isolated building units were studied, there is clearly scope for further computational studies, especially with regard to the effect of the solvent. Secondly, it has to be re-emphasized that there are many cases where the energy differences between several arrangements having a given composition are fairly small (often below 5 kJ mol^{-1}). Therefore, different local environments are likely to coexist within a crystal, and one should not be misled to expect that any of the building units shown in Figures 5 and 6 would correspond to the exclusively occurring arrangement within a real zeolite. A coexistence of different arrangements is indeed found experimentally, where up to three distinct ^{19}F NMR signals have been observed in (Si,Ge)-STW with intermediate Ge contents, with two of these signals corresponding to several possible arrangements.[13]

As a final remark to this section, we compare the present results to the earlier force field based calculations by Sastre and co-workers.[26] Their calculations for AST models containing 2, 3, and 4 Ge atoms in one *d4r* unit delivered a completely different energetic ordering: For each case, systems having no Ge-O-Ge link at all were found to be the energetically favored configurations (AST_(6Si,2Ge)_C_{2v}_0GeGe, AST_(5Si,3Ge)_C_{3v}_0GeGe, and AST_(4Si,4Ge)_T_d_0GeGe in the nomenclature of the present work). These models also exhibited the shortest Ge-F distances (with 1.9 to 2.0 Å). On the other hand, DFT-based predictions of the ^{19}F-NMR shifts agreed best with experimental observations for the AST_(6Si,2Ge)_C_{2v}_1GeGe, AST_(5Si,3Ge)_C_s_2GeGe, and AST_(4Si,4Ge)_D_{2h}_2GeGe models. Interestingly, the former two are the lowest-energy configurations for the respective compositions in the present study. Because these arrangements appeared thermodynamically unlikely on the basis of the force field calculations, Sastre and co-workers attributed the apparent preference to form *d4r* cages with Ge-O-Ge linkages to kinetic effects. However, the present DFT results indicate that the energetic ordering obtained in the force field calculations may be unreliable.

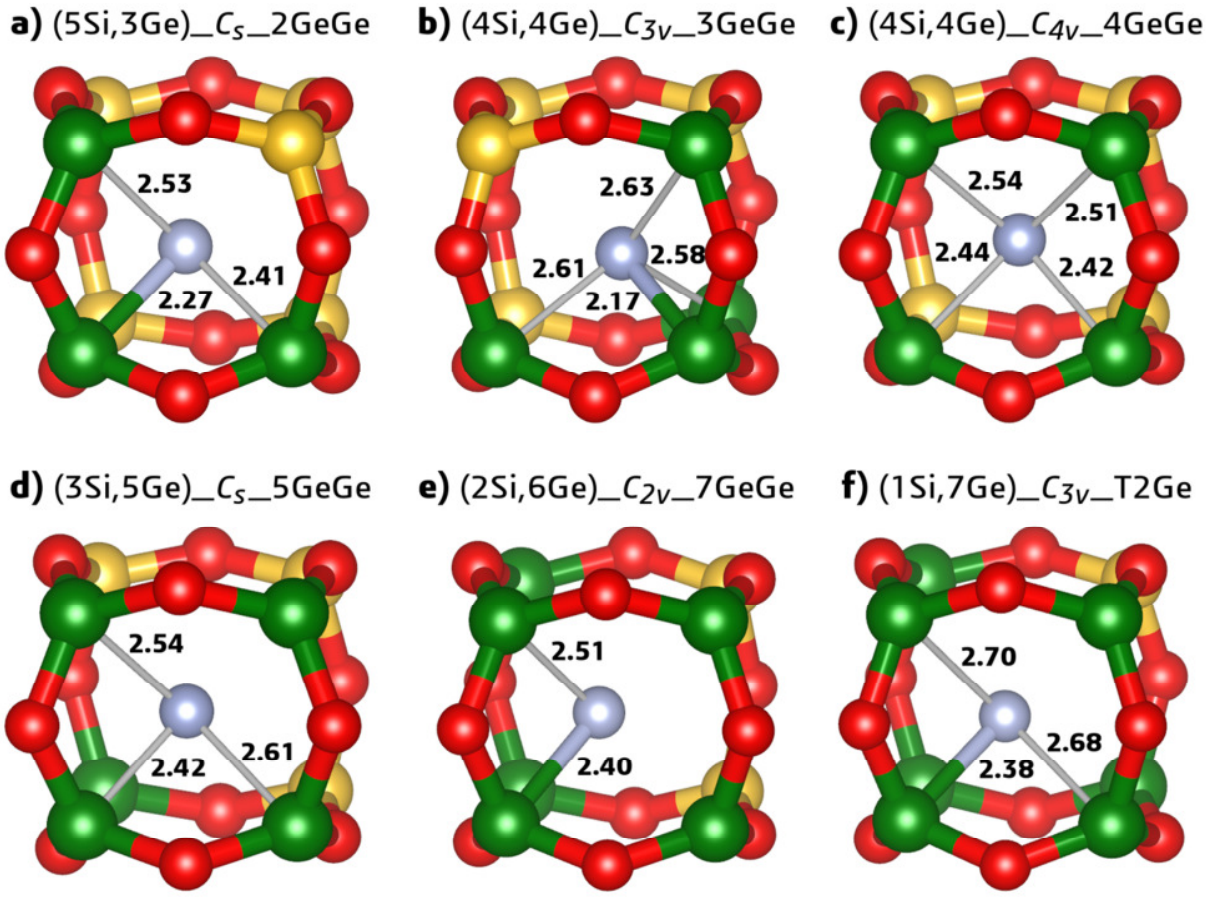

Figure 6. Fluoride environment in energetically preferred (TMA,F)-AST structures for n(Ge) = 0.3, 0.4 (where two structures are very close in energy), 0.5, 0.6, and 0.9. Selected interatomic distances are given in Å.

Table 2. Summary of results of DFT optimizations for models with different Ge contents and Ge arrangements. ΔE_{DFT} gives the energy difference with respect to the energetically most favorable model for a given composition (per *d4r* unit). *d*(Ge-F) corresponds to the shortest Ge-F distance. $Ge(Ge)_3/Ge(Ge)_2/Ge(Ge)_1/Ge(Ge)_0$ gives the number of Ge atoms that are surrounded by three/two/one/no Ge-O-Ge linkages within one *d4r* unit.

				(TMA,F)-AST		Template-free AST
	n(Ge)	T2	$Ge(Ge)_3/Ge(Ge)_2$ $/Ge(Ge)_1/Ge(Ge)_0$	*d*(Ge-F) / Å	ΔE_{DFT} / kJ mol^{-1}	ΔE_{DFT} / kJ mol^{-1}
SiO_2-AST	0	Si	-	-	-	-
AST_(7Si,1Ge)_C_{3v}	0.1	Si	0/0/0/1	2.20	-	-
AST_(6Si,2Ge)_C_{2v}_1GeGe	0.2	Si	0/0/2/0	2.26	**0.0**	6.0
AST_(6Si,2Ge)_C_{2v}_0GeGe	0.2	Si	0/0/0/2	2.45	9.8	5.0
AST_(6Si,2Ge)_D_{3d}_0GeGe	0.2	Si	0/0/0/2	2.61	13.2	**0.0**
AST_(5Si,3Ge)_C_s_2GeGe	0.3	Si	0/2/1/0	2.27	**0.0**	**0.0**
AST_(5Si,3Ge)_C_s_1GeGe	0.3	Si	0/0/2/1	2.22	5.3	2.6
AST_(5Si,3Ge)_C_{3v}_0GeGe	0.3	Si	0/0/0/3	2.53	13.0	4.0
AST_(4Si,4Ge)_C_{4v}_4GeGe	0.4	Si	0/4/0/0	2.42	0.2	6.3
AST_(4Si,4Ge)_C_{3v}_3GeGe	0.4	Si	1/0/3/0	2.17	**0.0**	8.1
AST_(4Si,4Ge)_C_2_3GeGe	0.4	Si	0/2/2/0	2.31	2.6	**0.0**
AST_(4Si,4Ge)_D_{2h}_2GeGe	0.4	Si	0/0/4/0	2.64	14.0	2.3
AST_(4Si,4Ge)_C_s_2GeGe	0.4	Si	0/1/2/1	2.42	7.2	4.1
AST_(4Si,4Ge)_T_d_0GeGe	0.4	Si	0/0/0/4	2.58	16.8	8.2
AST_(3Si,5Ge)_C_s_5GeGe	0.5	Si	1/3/1/0	2.42	**0.0**	5.5
AST_(3Si,5Ge)_C_s_4GeGe	0.5	Si	0/3/2/0	2.50	6.4	3.4
AST_(3Si,5Ge)_C_{3v}_3GeGe	0.5	Si	1/0/3/1	2.39	5.3	8.0
AST_(5Si,3Ge)_C_s_2GeGe_T2Ge	0.5	Ge	0/2/1/0	2.27	5.4	1.5
AST_(5Si,3Ge)_C_s_1GeGe_T2Ge	0.5	Ge	0/0/2/1	2.21	11.4	**0.0**
AST_(5Si,3Ge)_C_{3v}_0GeGe_T2Ge	0.5	Ge	0/0/0/3	2.52	20.7	2.8
AST_(2Si,6Ge)_C_{2v}_7GeGe	0.6	Si	2/4/0/0	2.40	**0.0**	5.1
AST_(2Si,6Ge)_C_{2v}_6GeGe	0.6	Si	2/2/2/0	2.50	1.9	6.9
AST_(2Si,6Ge)_D_{3d}_6GeGe	0.6	Si	0/6/0/0	2.70	6.6	4.0
AST_(4Si,4Ge)_C_{4v}_4GeGe_T2Ge	0.6	Ge	0/4/0/0	2.37	1.0	4.0
AST_(4Si,4Ge)_C_{3v}_3GeGe_T2Ge	0.6	Ge	1/0/3/0	2.18	1.2	4.0
AST_(4Si,4Ge)_C_2_3GeGe_T2Ge	0.6	Ge	0/2/2/0	2.32	3.3	**0.0**
AST_(4Si,4Ge)_D_{2h}_2GeGe_T2Ge	0.6	Ge	0/0/4/0	2.66	17.1	1.6
AST_(4Si,4Ge)_C_s_2GeGe_T2Ge	0.6	Ge	0/1/2/1	2.47	9.3	1.3
AST_(4Si,4Ge)_T_d_0GeGe_T2Ge	0.6	Ge	0/0/0/4	2.67	21.2	8.7
AST_(1Si,7Ge)_C_{3v}	0.7	Si	4/3/0/0	2.47	1.5	6.4
AST_(3Si,5Ge)_C_s_5GeGe_T2Ge	0.7	Ge	1/3/1/0	2.40	**0.0**	3.4
AST_(3Si,5Ge)_C_s_4GeGe_T2Ge	0.7	Ge	0/3/2/0	2.39	5.5	**0.0**
AST_(3Si,5Ge)_C_{3v}_3GeGe_T2Ge	0.7	Ge	1/0/3/1	2.30	3.5	5.6
AST_(0Si,8Ge)_O_h_T2Si	0.8	Si	8/0/0/0	2.77	2.7	5.4
AST_(2Si,6Ge)_C_{2v}_7GeGe_T2Ge	0.8	Ge	2/4/0/0	2.33	**0.0**	1.7
AST_(2Si,6Ge)_C_{2v}_6GeGe _T2Ge	0.8	Ge	2/2/2/0	2.44	3.8	3.4
AST_(2Si,6Ge)_D_{3d}_6GeGe _T2Ge	0.8	Ge	0/6/0/0	2.69	8.2	**0.0**
AST_(1Si,7Ge)_C_{3v} _T2Ge	0.9	Ge	4/3/0/0	2.38	-	
GeO_2-AST	1.0	Ge	8/0/0/0	2.81	-	

3.3 Equilibrium structures of template-free AST across the compositional range

Many previous computational studies of the relative stability of different Ge arrangements in silicogermanates have exclusively investigated models of the bare zeolite frameworks, without considering the influence of organic templates and fluoride anions on the energetic ordering.[18–20] This is a significant simplification, since the more likely configurations in calcined samples will correspond to those that are energetically favored in the as-synthesized material, unless a rearrangement of the T atoms occurs upon template removal (which appears unlikely). As a consequence, it is interesting to assess whether the energetic ordering changes when then non-framework species are removed from the structure models. The energy differences ΔE_{DFT} obtained for models of the bare AST framework are included in Table 2. First of all, it is worth noting that the range of ΔE_{DFT} values for a given composition is considerably smaller for template-free framework models: The difference between the most and least favorable arrangements never exceeds 9 kJ mol^{-1} (per *d4r* unit), whereas it amounts to more than 20 kJ mol^{-1} for some Ge contents in the case of (TMA,F)-AST. Secondly, the energetic ordering changes for all compositions except n(Ge) = 0.3. In particular, models with T2 = Ge are now favored from n(Ge) = 0.5 onwards. An inspection of the unit cell volumes (SI, Figure S1) shows that these models have systematically smaller volumes than those with T2 = Si. In contrast, the volume of the (TMA,F)-AST systems increases with Ge content, but does not vary appreciably for a given composition. Unlike for the template-containing systems, where (Si,Ge) arrangements having a larger number of Ge-O-Ge linkages are preferred, there is no such clear trend for the template-free models. Taken together, it can be concluded that the presence of fluoride anions and organic templates has a significant impact on the relative stability of different (Si,Ge) arrangements. Therefore, some caution should be exercised in the interpretation of computational results obtained for template-free models.

3.4 Dynamics of fluoride anions confined to *d4r* cages

As shown in the previous parts, the presence of localized Ge-F bonds depends on the heterogeneity of the environment. One might now wonder whether there could be several coexisting local minima for fluoride inside the cage, e.g. one at the center and another one in the proximity of a Ge atom, only one of which would be found in a static DFT optimization. In order to sample a significant part of the potential energy surface, constrained optimizations were performed in which the position of fluoride was varied along the body diagonal of the *d4r* cage. These optimizations were performed for SiO_2-AST, GeO_2-AST and AST_(7Si,1Ge)_C_{3v}, starting from the DFT-optimized structures. The coordinates of the atoms forming vertices and edges of the cage were optimized, whereas those of fluoride and of all other framework and non-framework atoms were held fixed. The resulting potential energy curves are shown in Figure 7 a. For both SiO_2-AST and GeO_2-AST, the energy minimum is located at the center of the cage, and the energy increases smoothly when moving towards a corner. There is a good correspondence between the potential energy curve obtained for SiO_2-AST and that calculated by Goesten et al. for fluoride at the center of a silsesquioxane model of a *d4r* unit.[54] The potential well is somewhat wider for GeO_2-AST than for SiO_2-AST due to the larger dimensions of the *d4r* cage. For AST_(7Si,1Ge)_C_{3v}, an asymmetric potential energy curve is found, with an energy minimum that is located at a distance of ~2.2 Å from the germanium atom, in accordance with the Ge-F distance obtained from the optimization. If fluoride is placed at the center of the cage, the energy is about 8 kJ mol^{-1} higher, and there are no indications for a secondary local minimum at the center (or elsewhere along the body diagonal).

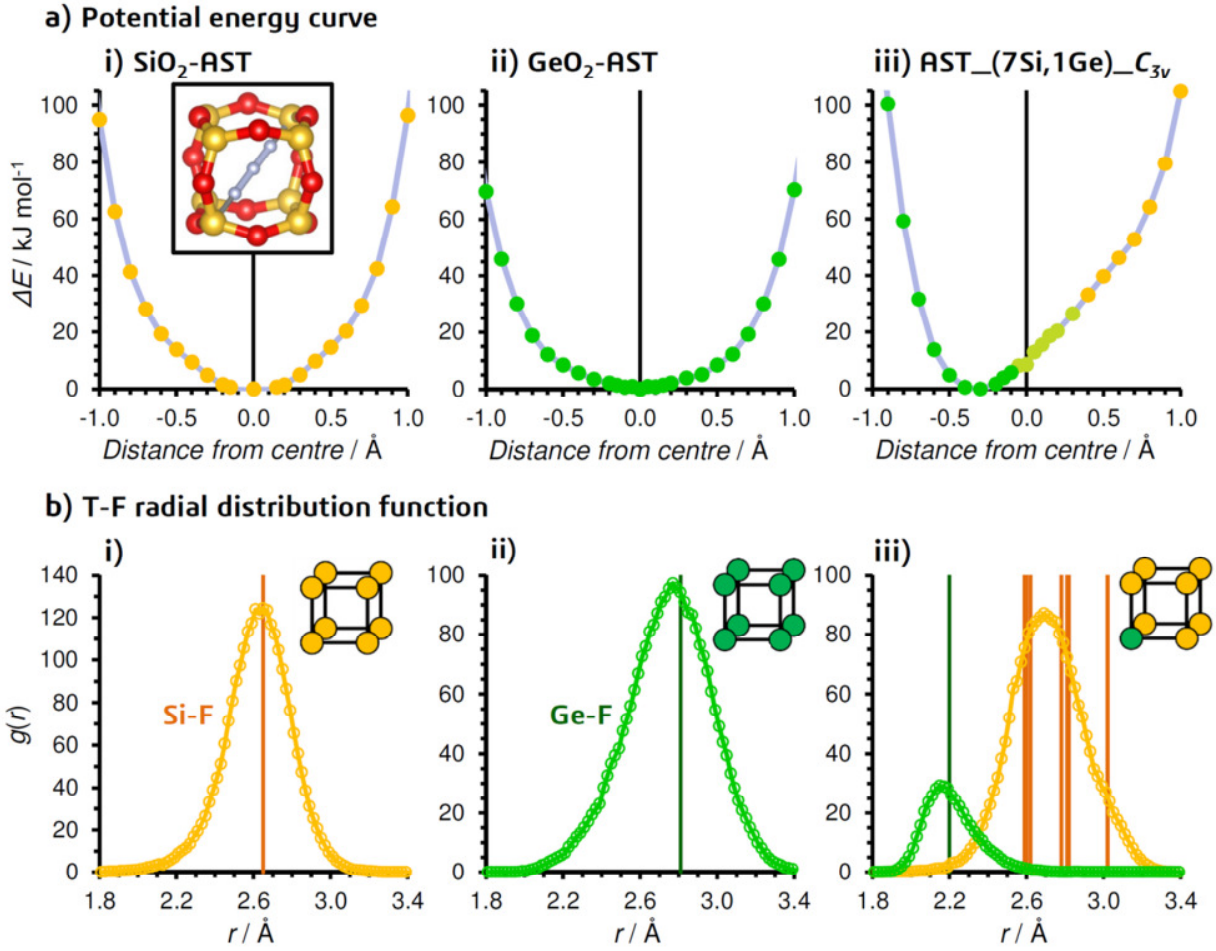

Figure 7 Top: Potential energy curve for a displacement of fluoride along the body diagonal of the *d4r* cage in SiO_2-AST, GeO_2-AST, and AST_(7Si,1Ge)_C_{3v}. Bottom: T-F radial distribution functions for the same three systems. Vertical lines indicate T-F distances in the DFT-optimized structures.

In order to sample the potential energy surface more comprehensively, *ab-initio* MD simulations were performed for the systems visualized in Figures 3, 5, and 6, thus, at least one model was considered for each composition of the *d4r* cage from (8Si,0Ge) to (0Si,8Ge). To start with, the root mean square displacements were evaluated for all elements (note that the RMSDs were calculated using the average coordinates from the 7.5 ps trajectories as reference). The RMSDs obtained for SiO_2-AST, GeO_2-AST, and AST_(7Si,1Ge)_C_{3v} are compiled in Table 3. For the T atoms, a slightly larger RMSD is found for Ge in GeO_2-AST (0.17 Å) compared to Si in SiO_2-AST (0.14 Å), despite the larger mass of germanium. This can be explained with the lower rigidity of Ge-O bonds compared to Si-O bonds, leading to an increased

freedom of motion of the atoms at the center of the TO_4 tetrahedra. For oxygen, the RMSDs are essentially identical for all three models (0.22 Å), as one would expect for isostructural systems. Very pronounced differences among the three systems are found for fluoride: For SiO_2-AST, the RMSD of 0.28 Å reflects the larger freedom of motion of the tetrel-bonded fluoride anions as compared to the (slightly lighter) oxygen atoms, which are held in place through directional Si-O bonds. The increased RMSD of fluoride in GeO_2-AST of 0.36 Å can be attributed to the larger dimensions of the *d4r* cage, permitting larger displacements from the cage center, in line with the wider potential well found above. For AST_(7Si,1Ge)_C_{3v}, where fluoride participates in a Ge-F bond, the RMSD is decreased to 0.22 Å, thus being virtually the same as for the oxygen atoms. This clearly shows that the fluoride anions lose a significant portion of their freedom of motion upon formation of Ge-F bonds, corroborating the localized (partly covalent) nature of these bonds. With regard to the TMA molecules, the RMSD of the nitrogen atoms is only moderately larger than that of fluoride confined to *d4r* cages, whereas the RMSDs of C and H atoms are much larger. As the nitrogen atom constitutes the center of mass of the TMA molecule, its small RMSD indicates that the overall displacement of the TMA molecules within the *ast* cages is only modest. The increased RMSDs of the atoms belonging to the methyl "arms" can be attributed to rotations of the TMA molecule about its center of mass. The larger dimensions of the *ast* cage in GeO_2-AST as compared to SiO_2-AST lead to an increased motion of the TMA molecules, reflected by systematically larger RMSDs.

Table 3. Root mean square displacements of all elements present in (TMA,F)-AST as obtained from MD calculations.

	SiO_2-AST *RMSD* / Å	GeO_2-AST *RMSD* / Å	AST_(7Si,1Ge)_C_{3v} *RMSD* / Å
Si	0.14 +/- 0.02	-	0.14 +/- 0.02
Ge	-	0.17 +/- 0.02	0.14 +/- 0.02
O	0.22 +/- 0.02	0.22 +/- 0.02	0.23 +/- 0.02
F	0.28 +/- 0.04	0.36 +/- 0.05	0.22 +/- 0.04
C	0.96 +/- 0.12	1.07 +/- 0.12	0.91 +/- 0.15
N	0.33 +/- 0.05	0.40 +/- 0.06	0.31 +/- 0.05
H	1.32 +/- 0.17	1.46 +/- 0.17	1.25 +/- 0.21

The RMSDs for other mixed (Si,Ge) systems are compiled in the SI (Table S3). As the analysis of the RMSDs of the other elements reveals no trends apart from those already mentioned, the following discussion will focus on the RMSD of fluoride anions, shown in Table 4. For the three systems with *n*(Ge) = 0.2, the RMSD varies from 0.23 Å for AST_(6Si,2Ge)_C_{2v}_1GeGe, the system having a localized Ge-F bond with *d*(Ge-F) = 2.26 Å, to 0.32 Å for AST_(6Si,2Ge)_D_{3d}_0GeGe, where fluoride resides almost at the cage center (Figure 5 c). This evolution agrees with the trend identified in the previous paragraph, and one might now expect that the reduction of the freedom of motion of fluoride is an entirely "local" phenomenon that depends solely on the interaction with the closest germanium atom. However, when plotting the values for all systems compiled in Table 4 against the shortest Ge-F distance (SI – Figure S2), it is apparent that there is no perfect correlation, as there are some systems where the RMSDs are much larger than what would be expected from the shortest Ge-F distance. In contrast, an alternative plot that uses the average Ge-F distance, calculated over all *x* Ge-F contacts within the ((8-*x*)Si,*x*Ge) *d4r* unit, shows a near-perfect correlation for all systems (Figure S2). Thus, the freedom of motion of fluoride depends not only on the nearest neighboring Ge atom in the equilibrium structure, but also on the presence of, and distance to, other Ge atoms in the *d4r* cage: When there is only one short Ge-F contact, or two Ge-F contacts that are similarly short, as in AST_(6Si,2Ge)_C_{2v}_1GeGe, fluoride remains rather confined to its equilibrium position at the temperature considered, with an RMSD that hardly exceeds that of strongly bonded framework oxygen atoms. However, when there are additional germanium atoms that are further away, attractive secondary interactions with these atoms cause a more dynamic behavior.

Table 4. Shortest and average Ge-F distances (from static DFT optimizations), median Ge-F distances, RMSDs of fluoride anions (from MD simulations). The error in the median Ge-F distances is estimated to be +/-0.02 Å.

		DFT optimizations		MD simulations	
	n(Ge)	Shortest *d*(Ge-F) / Å	Average *d*(Ge-F) / Å	Median *d*(Ge-F) / Å	*RMSD*(F) / Å
SiO_2-AST	0.0	-	-	-	0.28 +/- 0.04
AST_(7Si,1Ge)_C_{3v}	0.1	2.20	2.20	2.20	0.22 +/- 0.04
AST_(6Si,2Ge)_C_{2v}_1GeGe	0.2	2.26	2.28	2.30	0.23 +/- 0.04
AST_(6Si,2Ge)_C_{2v}_0GeGe	0.2	2.45	2.50	2.46	0.27 +/- 0.04
AST_(6Si,2Ge)_D_{3d}_0GeGe	0.2	2.61	2.66	2.64	0.32 +/- 0.05
AST_(5Si,3Ge)_C_s_2GeGe	0.3	2.27	2.40	2.42	0.25 +/- 0.04
AST_(4Si,4Ge)_C_{4v}_4GeGe	0.4	2.42	2.48	2.50	0.26 +/- 0.04
AST_(4Si,4Ge)_C_{3v}_3GeGe	0.4	2.17	2.50	2.53	0.26 +/- 0.04
AST_(3Si,5Ge)_C_s_5GeGe	0.5	2.42	2.62	2.59	0.28 +/- 0.04
AST_(2Si,6Ge)_C_{2v}_7GeGe	0.6	2.40	2.69	2.67	0.29 +/- 0.04
AST_(1Si,7Ge)_C_{3v} _T2Ge	0.9	2.38	2.76	2.74	0.32 +/- 0.05
GeO_2-AST	1.0	2.81	2.81	2.78	0.36 +/- 0.05

The first peaks in the T-F radial distribution functions $g(r)$, which correspond to the distances between the fluoride anion in a *d4r* cage and the T atoms at the cage vertices, are shown in Figures 7 b, 8, and 9 (the RDFs were always normalized in a way that the cumulative $g(r)$ for the first maximum corresponds to the number of Si or Ge atoms at the vertices of the cage). Furthermore, the median Ge-F distances, which mark the separation between the lower and upper 50% of the Ge-F distances within the first peak, are included in Table 4. First of all, it is worth pointing out that the median Ge-F distances obtained from the MD calculations are always within 0.04 Å of the average *d*(Ge-F) value measured in the DFT-optimized structures. If there were some cases in which fluoride anions moved from one local minimum to another one during the MD run, and remained confined to that minimum for a longer period of time, it could be expected that there were more pronounced deviations between the two values.

The RDFs of SiO_2-AST and GeO_2-AST, shown in Figure 7 b, reveal an essentially symmetric distribution of the T-F distances around a maximum value that coincides with the equilibrium distance in the DFT-optimized structures. As expected from the larger cage dimensions and the wider potential well, the RDF peak for GeO_2-AST is broader than for SiO_2-AST. On the side of short T-F distances, however, both

curves resemble each other, and T-F distances below 2.3 Å are essentially absent in both of them. In agreement with the findings from the static calculations, there are no indications for short Ge-F bonds in the pure-GeO_2 system. An inspection of the evolution of some T-F distances with time, shown for one selected fluoride anion in the Supporting Information (Figures S3 and S4), reveals that T-F distances below 2.3 Å do occur in both SiO_2- and GeO_2-AST. However, such close contacts are always very short-lived, and the fluoride anions move back towards a more central position within a few tenths of a picosecond. An additional piece of information that can be extracted from the MD trajectories is the flexibility of the T-O bonds, which can be inferred from the Si-O and Ge-O RDFs. These are shown in Figure S7. The fact that the Ge-O RDF is somewhat wider than the Si-O RDF indicates an increased flexibility of the Ge-O bonds, in line with the conclusion drawn above from the RMSDs of Si and Ge.

For the case of AST_(7Si,1Ge)_C_{3v}, also shown in Figure 7 b, there are two well-separated peaks for the Ge-F and Si-F distances in the RDF, with the position of the maxima corresponding to the (average) distances in the DFT-optimized structure. The Ge-F RDF has a rather sharp maximum, as one can expect from the presence of a localized bond that limits the freedom of motion. If there was a possibility for fluoride to relocate to a secondary local minimum at or near the cage center, one would expect a significant amount of Ge-F distances between of 2.6 to 2.7 Å, however, the value of $g(r)$ in this distance range is close to zero. Moreover, the curve falls to zero for Ge-F distances below 2.0 Å. Thus, the MD calculations provide no evidence for the existence of very short Ge-F bonds with a length of ~1.9 Å, which have been proposed in previous computational studies.[26,27] A plot of the T-F distances over time (Figure S5) corroborates both the absence of a local minimum at the cage center and the instability of short Ge-F bonds <2.0 Å.

Altogether, the results for the simplest systems permit us to conclude that there is only one local minimum for fluoride in each case, located at the cage center for the pure end members, and at a distance of about 2.2 Å from the Ge atom for AST_(7Si,1Ge)_C_{3v}. The situation becomes inevitably more complex – and less straightforward to analyze – when several corners of the *d4r* cage are occupied by germanium, where

a broadening of the RDF peaks will be caused by a combination of dynamic effects and the presence of different Ge-F distances. Nevertheless, the inspection of the RDFs can deliver useful insights. Figure 8 visualizes the RDFs for all three systems having 6 Si and 2 Ge atoms at the cage vertices. For the energetically preferred AST_(6Si,2Ge)_C_{2v}_1GeGe model, the T-F RDFs show no unusual features, with smooth distributions around the equilibrium T-F distances. As there are two similarly short Ge-F bonds in this system, a motion of fluoride towards either of the two Ge atoms will cause only a minor broadening of the $g(r)$ curve. In AST_(6Si,2Ge)_C_{2v}_0GeGe, the maximum is shifted towards shorter distances when compared to the equilibrium distances in the DFT-optimized structure, both of which are close to 2.5 Å. The rather large values of $g(r)$ between 2.1 and 2.3 Å indicate that there is a significant probability for fluoride to be displaced from its equilibrium position towards either of the two Ge atoms. The most interesting observations can be made for AST_(6Si,2Ge)_D_{3d}_0GeGe, where the Ge-F RDF exhibits one very broad maximum with similar $g(r)$ values from 2.2 to 2.9 Å (Figure 8 c), whereas the Si-F RDF has a narrower distribution that resembles that of SiO_2-AST. Apparently, the fluoride anions move primarily along the body diagonal connecting the two Ge atoms, while maintaining rather similar distances to the surrounding Si atoms. A plot of the Ge-F distances over time (Figure S6) shows a rapid exchange of the fluoride anions among the two Ge atoms at opposite corners of the cage. For this particular case, additional calculations of potential energy curves analogous to those presented in Figure 7 a were performed, considering displacements of the fluoride anion along the Ge-Ge body diagonal and along one of the Si-Si body diagonals. The resulting curves, shown in Figure S8, show a very shallow potential well along the Ge-Ge diagonal: A displacement from the center towards either of the Ge atoms by 0.3 Å incurs an energy increase of only ~2 kJ mol^{-1}, whereas a displacement of the same magnitude towards an Si atom leads to an increase of about 6 kJ mol^{-1}. This anisotropy of the potential energy surface explains the rather peculiar shape of the Ge-F RDF observed above. While the environment of the Ge atoms is identical to that in the system with only one Ge atom, AST_(7Si,1Ge)_C_{3v}, there are no local minima at Ge-F distances of ~2.2 Å. This indicates that the overall (Si,Ge) arrangement at the vertices of the *d4r* cage,

rather than the local environment of the Ge atoms, governs the relative stability of short Ge-F bonds compared to the center-of-cage position of fluoride.

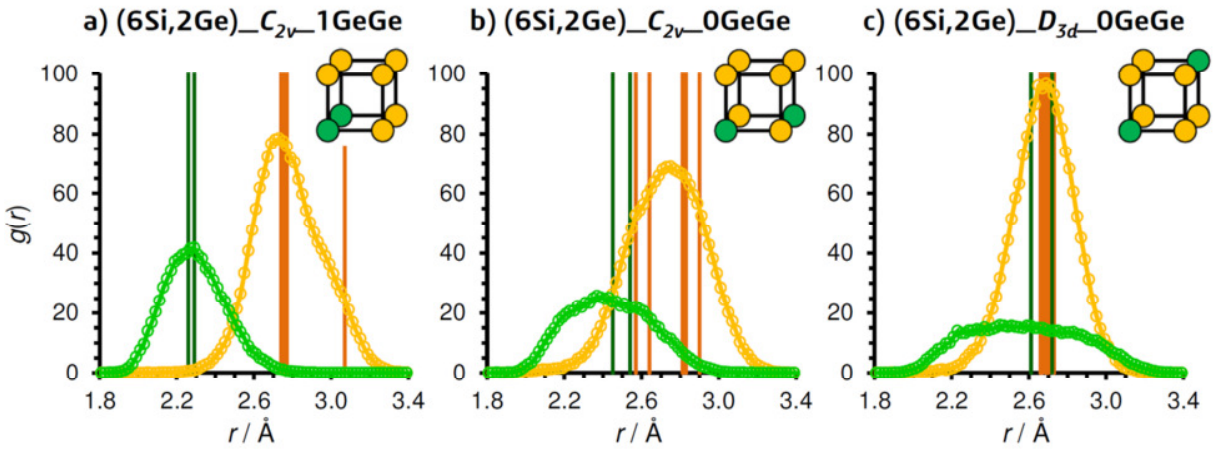

Figure 8. T-F RDFs for three (TMA,F)-AST models having *n*(Ge) = 0.2. Vertical lines indicate T-F distances in the DFT-optimized structures.

The radial distribution functions for systems with higher Ge contents are shown in Figure 9. Here, symmetric maxima in the Ge-F RDF appear for those systems where the distances between fluoride and germanium in the equilibrium structure are relatively similar, whereas the maxima for models having one or two short Ge-F contacts are asymmetric. Altogether, the radial distribution functions can be well described by assuming a statistic displacement of fluoride around its equilibrium position. Interestingly, even in the Ge-rich *d4r* cages, the average location of fluoride lies much closer to the Ge atoms than to the Si atoms: For example, the median Si-F distance in AST_(1Si,7Ge)_C_{3v} _T2Ge amounts to 2.98 Å, being almost 0.25 Å longer than the median Ge-F distance. In other words, the presence of a single Si atom at one of the vertices produces a significant anisotropy in the potential energy surface, which is pronounced enough to be clearly detectable even when the thermal motion of fluoride at 298 K is accounted for.

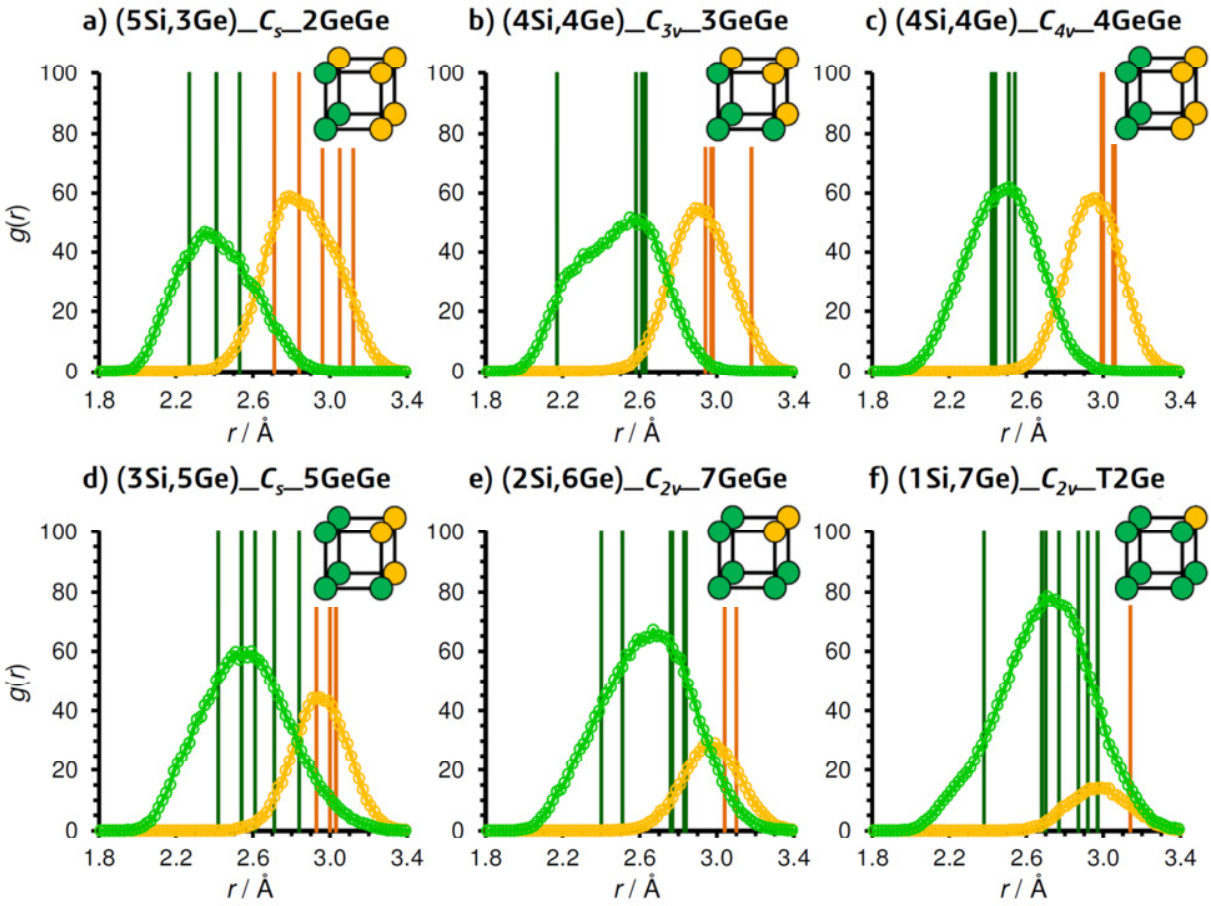

Figure 9. T-F RDFs for energetically preferred (TMA,F)-AST models having *n*(Ge) = 0.3, 0.4 (two models), 0.5, 0.6, and 0.9 (see Figure 6). Vertical lines indicate T-F distances in the DFT-optimized structures.

4. Concluding remarks

On the basis of the calculations presented above, the following conclusions can be drawn with regard to the preferred arrangements of Si and Ge at the *d4r* cages of AST frameworks, the equilibrium locations of fluoride, and its dynamic behavior: In fluoride-containing mixed (Si,Ge) systems, arrangements that maximize the number of Ge-O-Ge linkages are energetically favored. In the absence of fluoride, the computations predict a different energetic ordering without a clear trend. These findings strongly indicate that the presence of fluoride has a significant impact on the thermodynamically most stable (Si,Ge) arrangement, i.e. that there is a "templating effect". This may be particularly relevant for frameworks that

can be synthesized both in the presence and in the absence of fluoride anions, where the most probable local structure may differ depending on the synthesis route. There are, however, a few caveats in the interpretation of the DFT results: On the one hand, the complexity of the assembly process cannot be captured with DFT calculations for the periodic structure, and further work using a "bottom-up" approach would be needed to elucidate how thermodynamics and kinetics of the assembly affect the final structure. On the other hand, the energetic ordering of different distributions depends on the "deformability" of the T-O-T linkages in the structure, thus, on the framework type.[18,55] Therefore, the trends discussed above for AST are not necessarily valid for other frameworks with *d4r* building units. In this context, it is worth noting that EXAFS results indicated that Ge atoms preferentially locate at a single face of a (4Si,4Ge) *d4r* cage in IM-12 (UTL),[4] whereas a detailed NMR study showed that other arrangements are predominant in ITQ-13 and ITQ-22.[55]

With regard to the equilibrium position of fluoride, the calculations provide no evidence for the formation of pentacoordinated Ge atoms in GeO_2-AST, where fluoride resides at the center of the cage, as in SiO_2-AST. Formation of a relatively short Ge-F bond of ~2.2 Å occurs in (7Si,1Ge) *d4r* cages. Such short bonds are also prominent in *d4r* cages containing 2, 3, or 4 Ge atoms if the Ge atoms are located at neighboring vertices (many Ge-O-Ge linkages). At higher Ge contents, fluoride still tends to maintain shorter Ge-F than Si-F contacts, but there is no longer a formation of pentacoordinated germanium atoms. Neither DFT-based MD simulations nor calculations of the potential energy curve along the body diagonal of the *d4r* cage provide any indications for a coexistence of distinct local minima at the cage center and in the proximity of a Ge atom. By and large, the fluoride anions oscillate about the equilibrium positions obtained from the DFT optimizations at 298 K. Their freedom of motion, as measured through the RMSD, is correlated with the average Ge-F distance: If there is only a single Ge-F bond, the motion of fluoride is quite restricted, with an RMSD similar to that of the framework oxygen atoms, but if there are several Ge atoms in the vicinity, pairwise interactions with all these atoms lead to increased oscillations.

Altogether, the present study provides significant new insights into the local structure of fluoride-containing silicogermanate *d4r* units, insights that are not accessible through crystallographic methods, and may only be obtained indirectly via NMR spectroscopy or other spectroscopic methods. To this end, the results presented here should be of considerable value for future experimental studies of *d4r*-containing silicogermanate zeolites, e.g. in the context of an in-depth characterization of new materials obtained via hydrothermal or ADOR-based synthesis routes. In order to predict quantities that are directly measurable experimentally, we are currently working on a DFT-based prediction of the ^{19}F-NMR shifts for different (Si,Ge)-AST models. Going beyond the AST framework, future computational work should consider a range of framework types in order to assess the differences and common features of various silicogermanate zeolites.

With regard to the dynamics of fluoride anions under confinement, MD studies of related materials could deliver further insights. In all-silica zeolites that do not contain *d4r* units, fluoride is bonded to a single Si atom, forming SiO_4F trigonal bipyramids, with the Si-F bonds typically pointing into small cages.[56] Thus, it would be interesting to compare the fluoride dynamics in structures where fluoride resides in different building units. Other relevant groups of systems comprise fluoride-containing aluminosilicates[22] as well as alumino- and gallophosphates.[22,57] For gallophosphates containing *d4r* units, both a central position of fluoride (e.g. in LTA-type $GaPO_4$)[58] and off-center displacements towards two or three Ga atoms (e.g. in cloverite)[59] have been reported in X-ray crystallographic studies. As in the present work, DFT-based MD calculations could enhance our understanding of the dynamics of fluoride in these systems, especially whether a dynamic exchange occurs between different local minima in a cage.

Supporting information

Documentation of CP2K input and sample input files (in ZIP archive), DFT results for all-silica zeolites, additional figures and tables: Lattice parameters and unit cell volumes, RMSD values, T-O radial distribution functions, and selected interatomic distances from MD trajectories.

Acknowledgment

The author acknowledges funding by the Deutsche Forschungsgemeinschaft (DFG, German Research Foundation), project number 389577027 (FI 1800/5-1). Calculations were performed with resources provided by the North-German Supercomputing Alliance (HLRN), project hbc00030 (*Dynamics of fluoride anions in all-silica and silicogermanate zeolites*). The author thanks German Sastre and Reinhard X. Fischer for constructive comments on a first draft, and Ben Slater and Sanliang Ling for additional information concerning the TZVP basis sets from the CP2K MOLOPT_UCL library.

References

(1) Moliner, M.; Rey, F.; Corma, A. Towards the Rational Design of Efficient Organic Structure-Directing Agents for Zeolite Synthesis. *Angew. Chem. Int. Ed. Engl.* **2013**, *52*, 13880–13889.

(2) Sun, J.; Bonneau, C.; Cantín, A.; Corma, A.; Díaz-Cabañas, M. J.; Moliner, M.; Zhang, D.; Li, M.; Zou, X. The ITQ-37 Mesoporous Chiral Zeolite. *Nature* **2009**, *458*, 1154–1157.

(3) Jiang, J.; Jorda, J. L.; Diaz-Cabanas, M. J.; Yu, J.; Corma, A. The Synthesis of an Extra-Large-Pore Zeolite with Double Three-Ring Building Units and a Low Framework Density. *Angew. Chemie Int. Ed.* **2010**, *49*, 4986–4988.

(4) Verheyen, E.; Joos, L.; Van Havenbergh, K.; Breynaert, E.; Kasian, N.; Gobechiya, E.; Houthoofd, K.; Martineau, C.; Hinterstein, M.; Taulelle, F.; et al. Design of Zeolite by Inverse Sigma Transformation. *Nat. Mater.* **2012**, *11*, 1059–1064.

(5) Roth, W. J.; Nachtigall, P.; Morris, R. E.; Wheatley, P. S.; Seymour, V. R.; Ashbrook, S. E.; Chlubná, P.; Grajciar, L.; Položij, M.; Zukal, A.; et al. A Family of Zeolites with Controlled Pore Size Prepared Using a Top-down Method. *Nat. Chem.* **2013**, *5*, 628–633.

(6) Eliášová, P.; Opanasenko, M.; Wheatley, P. S.; Shamzhy, M.; Mazur, M.; Nachtigall, P.; Roth, W. J.; Morris, R. E.; Čejka, J. The ADOR Mechanism for the Synthesis of New Zeolites. *Chem. Soc. Rev.* **2015**, *44*, 7177–7206.

(7) Dawson, C. J.; Sanchez-Smith, R.; Rez, P.; O'Keeffe, M.; Treacy, M. M. J. Ab Initio Calculations of the Energy Dependence of Si–O–Si Angles in Silica and Ge–O–Ge Angles in Germania Crystalline Systems. *Chem. Mater.* **2014**, *26*, 1523–1527.

(8) O'Keeffe, M.; Yaghi, O. M. Germanate Zeolites: Contrasting the Behavior of Germanate and Silicate Structures Built from Cubic T_8O_{20} Units (T=Ge or Si). *Chem. - A Eur. J.* **1999**, *5*, 2796–2801.

(9) Sastre, G.; Pulido, A.; Corma, A. An Attempt to Predict and Rationalize Relative Stabilities and Preferential Germanium Location in Si/Ge Zeolites. *Microporous Mesoporous Mater.* **2005**, *82*, 159–163.

(10) Corma, A.; Navarro, M. T.; Rey, F.; Rius, J.; Valencia, S. Pure Polymorph C of Zeolite Beta Synthesized by Using Framework Isomorphous Substitution as a Structure-Directing Mechanism. *Angew. Chemie - Int. Ed.* **2001**, *40*, 2277–2280.

(11) Sastre, G.; Vidal-Moya, J. A.; Blasco, T.; Rius, J.; Jordá, J. L.; Navarro, M. T.; Rey, F.; Corma, A. Preferential Location of Ge Atoms in Polymorph C of Beta Zeolite (ITQ-17) and Their Structure-Directing Effect: A Computational, XRD, and NMR Spectroscopic Study. *Angew. Chemie - Int. Ed.* **2002**, *41*, 4722–4726.

(12) Blasco, T.; Corma, A.; Díaz-Cabañas, M. J.; Rey, F.; Rius, J.; Sastre, G.; Vidal-Moya, J. A. Synthesis, Characterization, and Framework Heteroatom Localization in ITQ-21. *J. Am. Chem. Soc.* **2004**, *126*, 13414–13423.

(13) Rigo, R. T.; Balestra, S. R. G.; Hamad, S.; Bueno-Perez, R.; Ruiz-Salvador, A. R.; Calero, S.; Camblor, M. A. The Si-Ge Substitutional Series in the Chiral STW Zeolite Structure Type. *J. Mater. Chem. A* **2018**, *6*, 15110–15122.

(14) Blasco, T.; Corma, A.; Díaz-Cabañas, M. J.; Rey, F.; Vidal-Moya, J. A.; Zicovich-Wilson, C. M. Preferential Location of Ge in the Double Four-Membered Ring Units of ITQ-7 Zolite. *J. Phys. Chem. B* **2002**, *106*, 2634–2642.

(15) Vidal-Moya, J. A.; Blasco, T.; Rey, F.; Corma, A.; Puche, M. Distribution of Fluorine and Germanium in a New Zeolite Structure ITQ-13 Studied by ^{19}F Nuclear Magnetic Resonance. *Chem. Mater.* **2003**, *15*, 3961–3963.

(16) Liu, X.; Chu, Y.; Wang, Q.; Wang, W.; Wang, C.; Xu, J.; Deng, F. Identification of Double Four-Ring Units in Germanosilicate ITQ-13 Zeolite by Solid-State NMR Spectroscopy. *Solid State Nucl. Magn. Reson.* **2017**, *87*, 1–9.

(17) Wang, Y.; Song, J.; Gies, H. The Substitution of Germanium for Silicon in AST-Type Zeolite. *Solid State Sci.* **2003**, *5*, 1421–1433.

(18) Kamakoti, P.; Barckholtz, T. A. Role of Germanium in the Formation of Double Four Rings in Zeolites. *J. Phys. Chem. C* **2007**, *111*, 3575–3583.

(19) Petkov, P. St.; Aleksandrov, H. A.; Valtchev, V.; Vayssilov, G. N. Framework Stability of Heteroatom-Substituted Forms of Extra-Large-Pore Ge-Silicate Molecular Sieves: The Case of ITQ-44. *Chem. Mater.* **2012**, *24*, 2509–2518.

(20) Odoh, S. O.; Deem, M. W.; Gagliardi, L. Preferential Location of Germanium in the UTL and IPC-2a Zeolites. *J. Phys. Chem. C* **2014**, *118*, 26939–26946.

(21) Whittleton, S. R.; Vicente, A.; Fernandez, C.; Rastegar, S. F.; Fishchuk, A. V; Sklenak, S. Effect of Ge/Si Substitutions on the Local Geometry of Si Framework Sites in Zeolites: A Combined High Resolution ^{29}Si MAS NMR and DFT/MM Study on Zeolite Beta Polymorph C (BEC). *Microporous Mesoporous Mater.* **2018**, *267*, 124–133.

(22) Caullet, P.; Paillaud, J.; Simon-Masseron, A.; Soulard, M.; Patarin, J. The Fluoride Route: A Strategy to Crystalline Porous Materials. *Comptes Rendus Chim.* **2005**, *8*, 245–266.

(23) Caullet, P.; Guth, J. L.; Hazm, J.; Lamblin, J. M.; Gies, H. Synthesis, Characterization and Crystal Structure of the New Clathrasil Phase Octadecasil. *Eur. J. Solid State Inorg. Chem.* **1991**, *28*, 345–361.

(24) Liu, X.; Ravon, U.; Tuel, A. Fluoride Removal from Double Four-Membered Ring (D4R) Units in As-Synthesized Ge-Containing Zeolites. *Chem. Mater.* **2011**, *23*, 5052–5057.

(25) Liu, X.; Ravon, U.; Bosselet, F.; Bergeret, G.; Tuel, A. Probing Ge Distribution in Zeolite Frameworks by Post-Synthesis Introduction of Fluoride in As-Made Materials. *Chem. Mater.* **2012**, *24*, 3016–3022.

(26) Pulido, A.; Sastre, G.; Corma, A. Computational Study of ^{19}F NMR Spectra of Double Four Ring-Containing Si/Ge-Zeolites. *ChemPhysChem* **2006**, *7*, 1092–1099.

(27) Sastre, G.; Pulido, A.; Corma, A. Pentacoordinated Germanium in AST Zeolite Synthesised in Fluoride Media. A ^{19}F NMR Validated Computational Study. *Chem. Commun.* **2005**, 2357–2359.

(28) Li, H.; Yaghi, O. M. Transformation of Germanium Dioxide to Microporous Germanate 4-Connected Nets. *J. Am. Chem. Soc.* **1998**, *120*, 10569–10570.

(29) Tang, L. Novel Framework Materials: Organically Templated Silicogermanates and Hybrid Fluorotitanates, PhD thesis, University of Stockholm, 2005.

(30) Villaescusa, L. A.; Lightfoot, P.; Morris, R. E. Synthesis and Structure of Fluoride-Containing GeO_2 Analogues of Zeolite Double Four-Ring Building Units. *Chem. Commun.* **2002**, 2220–2221.

(31) Yang, X. Synthesis and Crystal Structure of Tetramethylammonium Fluoride Octadecasil. *Mater. Res. Bull.* **2006**, *41*, 54–66.

(32) Corma, A.; Puche, M.; Rey, F.; Sankar, G.; Teat, S. J. A Zeolite Structure (ITQ-13) with Three Sets of Medium-Pore Crossing Channels Formed by 9- and 10-Rings. *Angew. Chemie - Int. Ed.* **2003**, *42*, 1156–1159.

(33) Song, J. Q.; Marler, B.; Gies, H. Synthesis of ITQ-7 with a New Template Molecule and Its Crystal Structure Analysis in the as Synthesized Form. *Comptes Rendus Chim.* **2005**, *8*, 341–352.

(34) Sastre, G.; Gale, J. D. Derivation of an Interatomic Potential for Fluoride-Containing Microporous Silicates and Germanates. *Chem. Mater.* **2005**, *17*, 730–740.

(35) Baerlocher, C.; McCusker, L. B. Database of Zeolite Structures. *http://www.iza-structure.org/databases/*, 2018.

(36) Anurova, N. A.; Blatov, V. A.; Ilyushin, G. D.; Proserpio, D. M. Natural Tilings for Zeolite-Type Frameworks. *J. Phys. Chem. C* **2010**, *114*, 10160–10170.

(37) Villaescusa, L. A.; Barrett, P. A.; Camblor, M. A. Calcination of Octadecasil: Fluoride Removal and Symmetry of the Pure SiO_2 Host. *Chem. Mater.* **1998**, *10*, 3966–3973.

(38) Okhotnikov, K.; Charpentier, T.; Cadars, S. Supercell Program: A Combinatorial Structure-Generation Approach for the Local-Level Modeling of Atomic Substitutions and Partial Occupancies in Crystals. *J. Cheminform.* **2016**, *8*, 17.

(39) Hutter, J.; Iannuzzi, M.; Schiffmann, F.; VandeVondele, J. CP2K: Atomistic Simulations of Condensed Matter Systems. *WIREs Comput. Mol. Sci.* **2014**, *4*, 15–25.

(40) VandeVondele, J.; Krack, M.; Mohamed, F.; Parrinello, M.; Chassaing, T.; Hutter, J. Quickstep: Fast and Accurate Density Functional Calculations Using a Mixed Gaussian and Plane Waves Approach. *Comput. Phys. Commun.* **2005**, *167*, 103–128.

(41) Perdew, J. P.; Burke, K.; Ernzerhof, M. Generalized Gradient Approximation Made Simple. *Phys. Rev. Lett.* **1996**, *77*, 3865–3868.

(42) Grimme, S.; Antony, J.; Ehrlich, S.; Krieg, H. A Consistent and Accurate Ab Initio Parametrization of Density Functional Dispersion Correction (DFT-D) for the 94 Elements H-Pu. *J. Chem. Phys.* **2010**, *132*, 154104.

(43) Krack, M. Pseudopotentials for H to Kr Optimized for Gradient-Corrected Exchange-Correlation Functionals. *Theor. Chem. Acc.* **2005**, *114*, 145–152.

(44) VandeVondele, J.; Hutter, J. Gaussian Basis Sets for Accurate Calculations on Molecular Systems in Gas and Condensed Phases. *J. Chem. Phys.* **2007**, *127*, 114105.

(45) Humphrey, W.; Dalke, A.; Schulten, K. VMD - Visual Molecular Dynamics. *J. Mol. Graph.* **1996**, *14*, 33–38.

(46) Fischer, M.; Evers, F. O.; Formalik, F.; Olejniczak, A. Benchmarking DFT-GGA Calculations for the Structure Optimisation of Neutral-Framework Zeotypes. *Theor. Chem. Acc.* **2016**, *135*, 257.

(47) Fischer, M.; Angel, R. J. Accurate Structures and Energetics of Neutral-Framework Zeotypes from Dispersion-Corrected DFT Calculations. *J. Chem. Phys.* **2017**, *146*, 174111.

(48) Román-Román, E. I.; Zicovich-Wilson, C. M. The Role of Long-Range van Der Waals Forces in the Relative Stability of SiO_2-Zeolites. *Chem. Phys. Lett.* **2015**, *619*, 109–114.

(49) Piccione, P. M.; Laberty, C.; Yang, S.; Camblor, M. A.; Navrotsky, A.; Davis, M. E. Thermochemistry of Pure-Silica Zeolites. *J. Phys. Chem. B* **2000**, *104*, 10001–10011.

(50) Li, Q.; Navrotsky, A.; Rey, F.; Corma, A. Thermochemistry of $(Ge_xSi_{1-x})O_2$ Zeolites. *Microporous Mesoporous Mater.* **2003**, *59*, 177–183.

(51) Bassindale, A. R.; Pourny, M.; Taylor, P. G.; Hursthouse, M. B.; Light, M. E. Fluoride-Ion Encapsulation within a Silsesquioxane Cage. *Angew. Chemie Int. Ed.* **2003**, *42*, 3488–3490.

(52) Taylor, P. G.; Bassindale, A. R.; El Aziz, Y.; Pourny, M.; Stevenson, R.; Hursthouse, M. B.; Coles, S. J. Further Studies of Fluoride Ion Entrapment in Octasilsesquioxane Cages; X-Ray Crystal Structure Studies and Factors That Affect Their Formation. *Dalt. Trans.* **2012**, *41*, 2048–2059.

(53) Bauzá, A.; Mooibroek, T. J.; Frontera, A. Tetrel-Bonding Interaction: Rediscovered Supramolecular Force? *Angew. Chemie Int. Ed.* **2013**, *52*, 12317–12321.

(54) Goesten, M. G.; Hoffmann, R.; Bickelhaupt, F. M.; Hensen, E. J. M. Eight-Coordinate Fluoride in a Silicate Double-Four-Ring. *Proc. Natl. Acad. Sci.* **2017**, *114*, 828–833.

(55) Kasian, N.; Tuel, A.; Verheyen, E.; Kirschhock, C. E. A.; Taulelle, F.; Martens, J. A. NMR Evidence for Specific Germanium Siting in IM-12 Zeolite. *Chem. Mater.* **2014**, *26*, 5556–5565.

(56) Pulido, A.; Corma, A.; Sastre, G. Computational Study of Location and Role of Fluoride in Zeolite Structures. *J. Phys. Chem. B* **2006**, *110*, 23951–23961.

(57) Loiseau, T.; Férey, G. Crystalline Oxyfluorinated Open-Framework Compounds: Silicates, Metal Phosphates, Metal Fluorides and Metal-Organic Frameworks (MOF). *J. Fluor. Chem.* **2007**, *128*, 413–422.

(58) Simmen, A.; Patarin, J.; Baerlocher, C. Rietveld Refinement of F-Containing $GaPO_4$-LTA. In *Proceedings from the Ninth International Zeolite Conference*; Elsevier, 1993; pp. 433–440.

(59) Estermann, M.; McCusker, L. B.; Baerlocher, C.; Merrouche, A.; Kessler, H. A Synthetic Gallophosphate Molecular Sieve with a 20-Tetrahedral-Atom Pore Opening. *Nature* **1991**, *352*, 320–323.